

RESEARCH PAPER

Experimental Investigation on Bond Stress Behavior of Sand-Coated GFRP Bars with Concrete

Zana M. Qader , Feirusha S. M. Kakshar

Department of Civil Engineering, College of Engineering, Salahaddin University-Erbil, Kurdistan-Iraq.

ABSTRACT:

In this paper, a comprehensive experimental study was conducted to investigate the bond performance of sand-coated glass fiber reinforced polymer (GFRP) bars embedded in normal concrete with different bar sizes and different embedded regions of concrete beams following the regulation of the Rilem beam. The achieved results are compared to the analytical equations presented by current codes and reputable recent research using the average bond strength and the free end bond stress-slip curves. This study contains the effect of bar size and embedded length on bond stress and slippage of sand-coated GFRP bars. From the data observed, bond stress of 8mm bar size is about 23% higher than 10mm and 16% higher than 12mm bar size for 10D embedded length. The 8mm bar size showed the maximum bond stress of 13.8MPa among all the other specimens while the maximum slip measurement was detected from a 12mm bar size of 1.519mm. Bond stress with beam test showed a higher value by almost twice than those derived from other codes. In general, as the bar size increases the bond stress decreases, and as the embedded length increases the bond stress tends to fall. Similarly, the slip of the bar rises as the embedded length rises. The embedded length of 10D recommended by RILEM 1994 is inadequate for GFRP bars. Finally, GFRP bars show higher bond stress than steel bars by 20%.

KEY WORDS: Bond stress, Slip, concrete beam, sand coated GFRP

DOI: <http://dx.doi.org/10.21271/ZJPAS.35.3.3>

ZJPAS (2023) , 35(3);30-38

1. INTRODUCTION:

Concrete reinforced with steel is the most popular structural material used in construction across the world. In some situations, however, it is commonly accepted that corrosion of steel reinforcement can cause structural parts to weaken or even collapse, costing a large cost for maintenance and reinforcing. In an effort to boost structural durability, the worldwide construction industry has utilized costly thick concrete coverings and extremely alkaline concretes on a massive scale. Cathodic protection, reinforcing with stainless steel, reinforcing with epoxy-coated steel, and other more contemporary solutions to the durability issue can all raise construction costs or complicate designs. Each year, hundreds of billions of dollars are spent on reinforcing and restoring concrete structures whose reinforcement has deteriorated as a result of corrosion, prompting researchers to focus on alternative options (Fernandez et al., 2016).

Over the past decade, reinforced concrete (RC) constructions have increasingly utilized fiber-reinforced polymer (FRP) reinforcement in place of conventional steel reinforcement. Nowadays, FRP reinforcement possesses exceptional nonmagnetic characteristics, competitive resistance, and low fatigue life. According to Reichenbach et al., (2021), the most prevalent kind of FRP reinforcement is GFRP and carbon fiber reinforced polymer (CFRP). GFRP bars differ dramatically from steel due to their significantly lower modulus of elasticity and their surface-preparation-dependent binding to concrete.

Due to the passage of tensile stress from the matrix of the concrete to the reinforcement, FRP-reinforced concrete requires a sufficient interfacial connection between the bars and the concrete for optimal performance. The increase in stress, which is reliant on chemical adhesion, bar

* Corresponding Author:

Zana M. Qader

E-mail: zana.qader@su.edu.krd

Article History:

Received: 17/08/2022

Accepted: 07/10/2022

Published: 15/06/2023

geometry, mechanical contact, compressive strength of concrete, and frictional forces, assures the bond-slip interaction between the concrete and FRP bar's surroundings (Lin and Zhang, 2014).

Coelho et al. (2015) utilized the beam test, direct pull-out test, ring pullout, and splice test to investigate the bond behavior of FRP reinforcement to concrete. In a reinforced concrete element, the configurations for the ring pullout and direct pullout tests do not correspond to the real bond circumstances (Kotynia et al., 2017). Consequently, only the beam test and splice test, as described by Basaran and Kalkan (2020), correctly depict the reinforcing bond stress behavior. The study on beam bonding tests using FRP reinforcement is insufficient.

Maranan et al.,(2014) reported that the pull-out resistance of GFRP bars embedded in geopolymer concrete with an average cylinder compressive strength of about 33.1 MPa was generally higher than that of GFRP bars embedded in concrete with normal strength. That is a result of the geopolymer concrete having a higher tensile strength than cement-based concrete.

There are some factors that have a huge influence on how well FRP reinforcement bonds to the concrete are the nominal diameter of the bars, surface texture, and embedded length. Utilizing FRP bars, which come in a variety of materials, sizes, and surface textures, is crucial today (Achillides and Pilakoutas, 2004). These are the main factors affecting the state in which the element will be used. The aforementioned parameters differ from one FRP type to another. In comparison to steel bars, FRP bars are available on different surface textures such as Grooved, Ribbed and Sand coated, etc. (Rolland et al., 2020).

The required overlap length and stress state of the GFRP bars seems unclear which is a gap in the research field on the FRP bars. Future work can be directed to find a modification factor for existing equations of bond stress.

Given all of the aforementioned reasons, this study presents the results of bond tests carried out using reinforcing GFRP bars, conducted according to the beam models. This research contributes to a) a better understanding of the GFRP bar-concrete bond; and b) providing key information for the definition of future standards for bond tests for reinforcing bars.

2. Experimental Works

Pull-out tests with the less embedded region and related techniques are traditionally used to examine the bond between reinforcing steel. Such tests, especially for non-standard reinforcing bar geometries, are not suitable for determining characteristic development lengths and behavior. For this purpose, ASTM A944, RILEM, and other standards require growth length tests, such as beam-end tests. The beam geometry was developed using the RILEM-1994 beam test recommendation as a guide.

This study tries to compare three bar diameters of sand-coated GFRP and three different embedded lengths, respectively. The specimens are set into three groups, each group supposed to contain three samples with three various embedded lengths. As shown in Fig. 2.



Fig. 1 Surface texture of the used sand-coated GFRP bars

Fig. 3 illustrates the general view of the arrangement of steel reinforcement of all the beams.



Fig. 2 Steel reinforcement of the beam specimens. The properties of the used materials concrete, sand-coated GFRP, and steel are represented in Table 1. The average cylindrical compressive strength of 21MPa is used as it was determined by using 150*300mm cylinders which is somehow equal to 25MPa with cubic compressive strength.

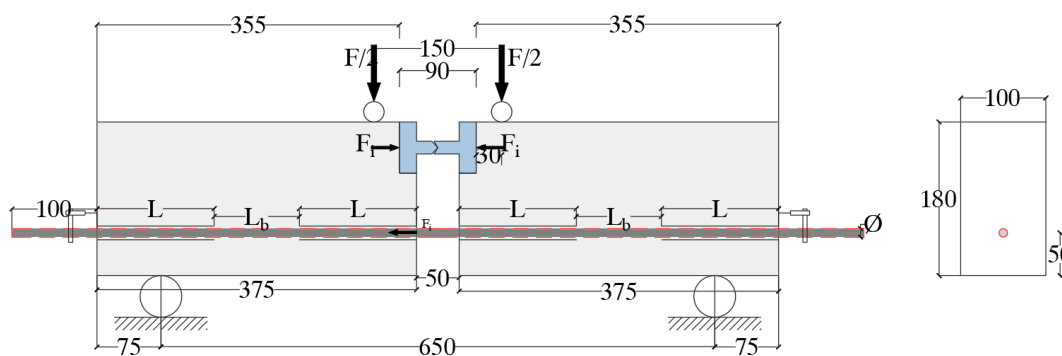
Table 1 The mechanical properties of concrete, GFRP bars, and steel bars

Material	Density (Kg/m ³)	Poisson's Ratio	Yield Tensile Strength (MPa)	Ultimate Tensile Strength (MPa)	Modulus of Elasticity (GPa)
Concrete	2400	0.18	-	-	22.2
Sand-Coated GFRP	1300	0.2	-	1100	47.5
STEEL	7850	0.3	420	620	200

3.Specimens

The proposed dimension of the tested beams was 650mm span (c/c of supports), 180mm height, and 100mm width. The beam is reinforced as the detail of Fig. 4 and with the main bar that works in bending of GFRP with the modulus of elasticity of 47.5GPa and ultimate strength of 1100MPa.

The beam specimen is used to measure the bonding stress of bars with an applicable embedded length of 5,10 and 15 times the diameter of the bar. Using a computerized universal machine of 150kN capacity, all specimens were exposed to the two-point load applied at the upper part near the center of the beam with half loads of $F/2$ (Fig. 4).



a




b

Fig. 3 a) Illustration of the geometry of the tested beam, b) Specimen under testing

Table 2 shows the grouping design, and the variables of the investigation studied in this paper.

Table 2 Design of the tested specimens

Specimen No.	Specimen ID	Bond Length	Diameter (mm)	Material
1	GS-8-5	5D	8	Glass 
2	GS-8-10	10D		
3	GS-8-15	15D		
4	GS-10-5	5D	10	
5	GS-10-10	10D		
6	GS-10-15	15D		
7	GS-12-5	5D	12	
8	GS-12-10	10D		
9	GS-12-15	15D		

4. Analysis Methods

To determine bond stress, numerous modern codes and recent scientific research offer their own modified equations that are derivable from Equation 1. This work presents the comparative investigation of bond stress between the results of the conducted experiment and the results obtained on the basis of the mentioned modified equations (Diab et al., 2014).

As shown in Fig. 1, the ultimate bond stress of the bar (τ_u) can be calculated using equation 1 as shear bond stress of the used bar over the length embedded inside concrete:

$$\tau_u = \frac{F_u}{\pi * D * L_b} \quad (1)$$

Where: F_u -the pullout force, D is nominal bar diameter and L_b -the embedded length.

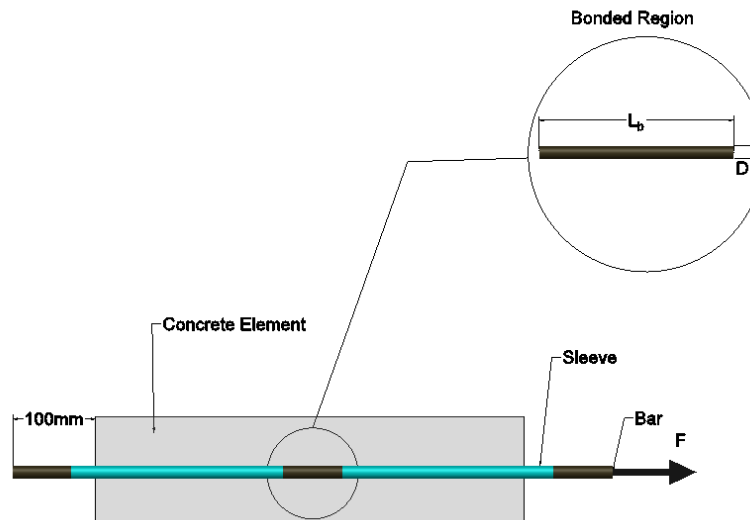


Fig. 4 Illustration of FRP bar inside concrete and bond length

Equation (2) can be used to calculate bond strength in accordance with CSA S806-12 (2012):

$$\tau = \frac{d_{cs} * \sqrt{f_c'}}{1.15 k_1 k_2 k_3 k_4 k_5 \pi D} \quad (2)$$

where d_{cs} is the shorter distance from the nearest concrete surface to the center of the bar being developed or two-thirds of the center-to-center spacing of the bars being developed (shall not be

taken greater than 2.5 times bar diameter D), measured in millimeters; this distance is not to exceed 2.5 times bar diameter D . where k_1 refers to the placement factor of the bar, k_2 to the density factor of the concrete, k_3 to the size factor of the bar, k_4 to the fiber factor of the bar, and k_5 to the surface profile factor of the bar. The highest value

of f_c' that is allowed, in accordance with CSA Standard S806-02, is 64 MPa (Mias et al., 2013).

Equation (3) can be used to determine bond strength in accordance with ACI 440.1R-15:

$$\tau = \left(0.33 + 0.025 * \frac{C}{D} + 8.3 * \frac{D}{l_e}\right) * \sqrt{f_c'} \quad (3)$$

where C is one-half of the center-on-center spacing of the bars that are being developed, l_e is the imbed length, and C/D should not be selected in such a way that it will take longer than 3.5 from the cover to the center of the bar.

Calculating the bond strength may be done using Equation (4) and Equation (5), respectively, as stated by Okelo and Yuan (2005) and Lee et al. (2008):

$$\tau = 14.7 \left(\frac{\sqrt{f_c'}}{D}\right) \quad (4)$$

$$\tau = 3.3f_c'^{0.3} \quad (5)$$

Table 3 Experimental and code predicted bond strength GFRP bars with concrete

Bar size (mm)	L_b (mm)	Peak Load (kN)	Axial Stress in GFRP bar (MPa)	Bond Stress (MPa)				
				Test Results	ACI440.1R-15	CSA-S806-02	(Okelo and Yuan, 2005)	(Lee et al., 2012)
8	40	15.954	317.56	15.87	9.52	3.963	8.42	8.22
	80	27.746	552.27	13.8	5.71			
	120	36.76	731.69	12.19	4.448			
10	50	18.079	230.31	11.51	9.52	3.96	6.73	8.22
	100	35.028	446.22	11.15	5.71			
	150	45.003	573.29	9.55	4.448			
12	60	29.58	261.68	13.079	9.52	3.96	5.61	8.22
	120	53.75	475.50	11.89	5.71			
	180	68.75	608.19	10.13	4.448			

Table 3 summarizes the comparison between the experimental bond strength of various specimens and estimates based on the methodologies described in ACI 440.1R-15, CSA S806-12 (Okelo and Yuan, 2005) and (Lee et al., 2012). For GFRP-reinforced specimens, it can be

5.Results and Discussion

Table 3 compares the empirically determined bond strengths from beam testing to those obtained from codes and other known formulas. According to CSA-S806-12, neither the strength of the concrete nor the size of the bars impacts the bond strength. Nonetheless, it can be deduced from the test findings that the diameter of the bar and the length of its embedment may influence the bond strength as well as concrete compressive strength which is not variable in this investigation. The analytical equations account for the impacts of improved confinement and tensile strength by including compressive strength as well as several characteristics, such as bar size and bonded area. In this study, the bond area length changes with bar diameters of 5, 10, and 15, which has a significant effect on peak load and bond stress.

observed that the ACI 440.1R code was more conventional and trustworthy than alternative methods. Table 3 revealed that bar diameter and embedment length did not influence bond strength as assessed by Canadian building codes. In addition, because the depth of the concrete under

the bars is less than 300 mm, the Canadian code disregards the influence of bar placement on bond strength. As seen in Table 3, the position of the bars does not affect the bond strength. Due to the Canadian code, the bond strength diminishes as embedment length grows according to ACI 440.1R. In the ACI 440.1R calculation for normalized concrete cover and embedment length, the influence of bar diameter on bond strength has been ignored. In addition, the ACI 440-1R code does not consider how surface configuration influences bond strength. The concrete strength range of 28–45 MPa served as the basis for the formulation of the ACI 440.1R equation. Therefore, it cannot be assumed that it will predict the bond strength of GFRP bars properly. Due to Canadian code constraints on concrete cover and strength, the expected bond strength is constant for all test specimens, as displayed. The bond strength calculated from Canadian design codes is lower than the experimentally determined minimum value; hence, the development time specified by these regulations is inadequate.

When comparing ACI 440.1R-15 results to experimental values, the results of GS-8-5, GS-8-10 and GS-8-15 are only 60%, 41%, and 36% of the experimental, respectively, which is a bit close for 5D but far away from 10D and 15D of bonded length, almost half of the results. The results of the experiments showed that for GS-10-5, GS-10-10, and GS-10-15, respectively, the percentages were 83%, 51%, and 47%, while for GS-12-5, GS-12-10, and GS-12-15, the corresponding percentages were 73%, 48%, and 44%. It can be conducted that the results of the experiment for 5D are the closest to those derived from ACI440.1R-15, this may due to the effect of surface texture, while the results obtained by (Lee et al., 2012) are consistent with the experimental results for bond length of 15D, however, (Lee et al., 2012) do not take the bonded length into account.

The axial stress of the sand-coated GFRP bars shows the applicability of the embedded length of the bars. Maximum stress reached about 67% of the ultimate axial stress. From the results of Table 3, all the bars failed due to pull-out mode failure. This demonstrates that none of the lengths 5D,

10D, and 15D will not be sufficient to fail the bar in axial stress.

As shown in Table 3, the peak load increased as the embedment length of 5D, 10D, and 15D increased. The percentage increase in loading for an 8mm bar with a 10D embedded length was 73.9 times the peak load for a 5D embedded length and 130 times the peak load for a 15D embedded length. Comparatively, the ratio of 5D to 10D and 15D for 10mm bars was 94% and 149%, respectively. Ultimately, the findings for the 12mm bar size indicated that 82% and 132% of 5D were greater than 10D and 15D. The maximum peak load was measured in a 12 mm bar (GS-12-15 beam specimen) with 68.75kN, while the lowest peak load was seen in an 8 mm bar with 15.954kN. (GS-8-5 beam specimen). It can be proved that when bar size grows, peak load and embedded length both rise.

Figure 5 depicts the relationship between bond stress and slippage for the sand-coated GFRP bar.

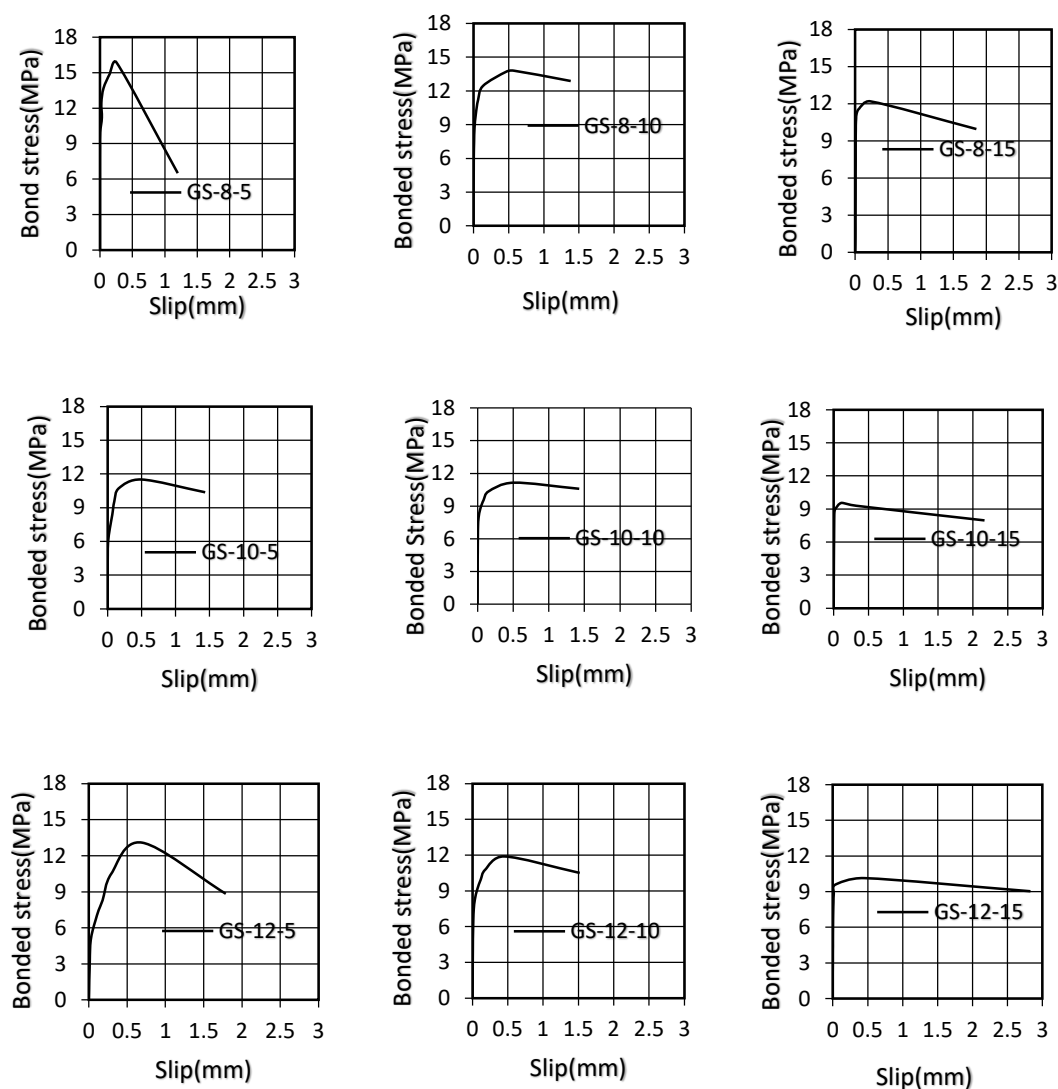


Fig. 5 Comparison of bond stress and slip for all specimens

Specimen GS-8-5 had maximum stress of 15.86MPa, while the maximum load caused the bar to slide at 0.255mm. GS-8-10 had maximum stress of 13.8MPa and a slip of 0.505mm, whereas GS-8-15 had maximum stress of 12.19MPa and a slip of 0.231mm. For beams GS-10-5 to GS-10-15, the maximum stress was 11.51, 11.15, and 9.55 MPa, while the slip was 0.405, 0.505, and 0.305mm, respectively. While the bond stress for GS-12-5 to GS-12-15 was 13.09, 11.89, and 10.13MPa, the slip was 0.69, 0.452, and 0.451mm, respectively. According to Table 4, the greatest slip reached 2.5mm for GS-12-15, while the smallest slip was 1.199mm for GS-8-5. Due to the distribution of shear stress around the perimeter of the bar, the slip tends to grow as the bar's diameter rises. Comparing the findings of ribbed GFRP bars to those of steel bars, as

detailed by (Tekle et al., 2020), steel bars exhibit a slightly higher bond stress value that is dependent on the surface roughness of the bar. For steel bars, there is no texture comparable to sand-coated FRP bars. Solyom and Balázs (2020) demonstrated in their study that the bond strength of all FRP bars was superior to that of steel bars. The results show that the bonding behavior of steel bars in self-compacted concrete is superior to that of GFRP bars when treated appropriately (Golafshani et al., 2014). According to the findings of a study conducted by Hasan Sahan Arel and Semsi Yazici, (2014), which compared the bond stress of a GFRP bar to that of a steel bar, it was discovered that the GFRP bar exhibited an improvement in bond stress that was 20% higher than the bond of steel bar due to the layer of epoxy of sand over the bars when applied to concrete with a compressive strength of 21MPa.

Figure 6 shows the bond stress versus embedded length

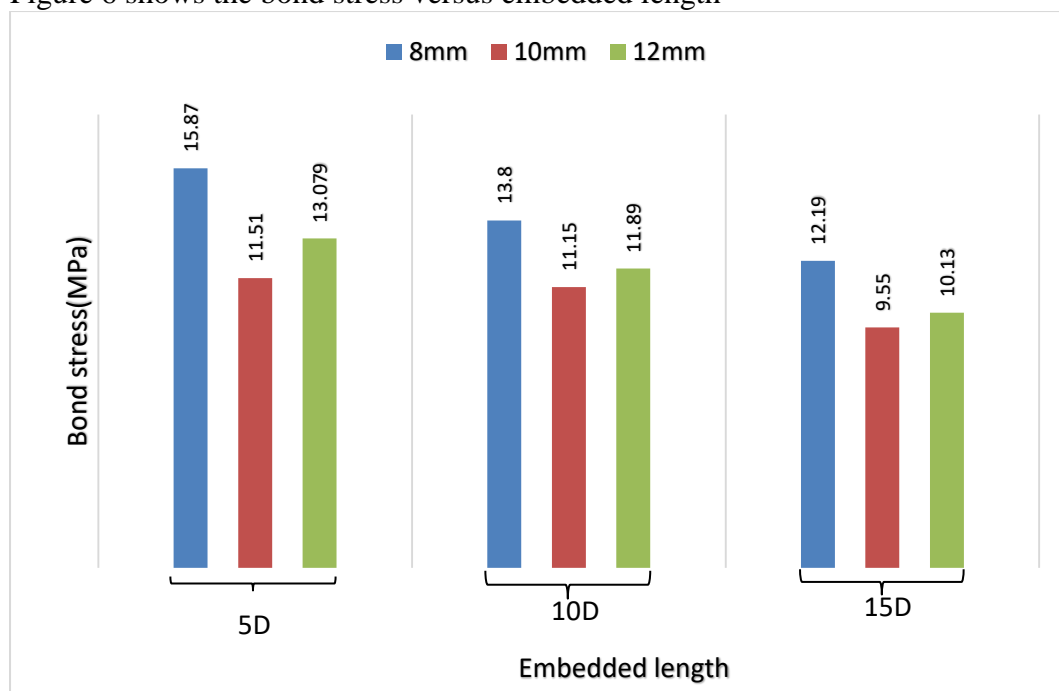


Fig. 6 The analysis of bond strength at various embedding lengths

From Fig.6 can be detected that the stress of 10mm bar is about 28% lower than those from 8mm and was 12% lower than 12mm bar for the embedded length of 5D while for 10D, the results of 10mm bar are about 20% and 6% lower than 8mm and 12mm, respectively. Also, comparing results of 15D the outcomes of 10mm bar were 22% and 28% for both 8mm and 12mm, respectively. In general, the bond stress appears to grow as the bar size decreases, however, the bond stress decreases as the embedding length increases due to the increase in surface area.

6. Conclusions

The results of experimental work and analytical equations led to the following conclusions:

- The sand-coated bar surface texture contributes significantly to the GFRP bars' advantageous binding behavior to concrete. There was evidence of pull-out failure in every sample. Sand grains separating from the GFRP's sand-coated surface caused the bond to collapse, and damage to the outer layer of the GFRP bars governed its occurrence.
- For the concrete compressive strengths examined here, the bond length of 10D, as recommended by RILEM, will not cause yielding or rupture of the GFRP bars for

strength 21 MPa. For these concrete strengths, the bond length shall be more than 10D.

- After normal concrete's bond stress peaked, the GFRP bars showed an instantaneous bond breakdown with a massive absence of bond resistance as the sand grains were stripped away.
- As the embedded length is increased, the bond stress associated with the ultimate peak load decreases significantly. The slip-free ends increase in proportion to the ultimate peak load, which was only 2.5mm, as the embedded length continues to extend.
- A decrease in bond strength occurs when there is an increase in both the embedment length and the bar diameter. When dealing with normal concrete specimens, increasing the bar size resulted in a decrease in the rate of bond strength.
- The estimates of bond strengths of sand-coated GFRP that are offered by the CSA-S806 code are considered to be more conservative than those offered by other codes.

- In general, increasing the bar size will decrease the bond stress for the same embedded length.

References

- Achillides, Z., Pilakoutas, K., 2004. Bond behavior of fiber reinforced polymer bars under direct pullout conditions. *J. Compos. Constr.* 8, 173–181.
- Basaran, B., Kalkan, I., 2020. Investigation on variables affecting bond strength between FRP reinforcing bar and concrete by modified hinged beam tests. *Compos. Struct.* 242, 112185.
- Coelho, M.R., Sena-Cruz, J.M., Neves, L.A., 2015. A review on the bond behavior of FRP NSM systems in concrete. *Constr. Build. Mater.* 93, 1157–1169.
- Diab, A.M., Elyamany, H.E., Hussein, M.A., Al Ashy, H.M., 2014. Bond behavior and assessment of design ultimate bond stress of normal and high strength concrete, *Alexandria Eng. J* 53, 355–371.
- Fernandez, I., Herrador, M.F., Marí, A.R., Bairán, J.M., 2016. Structural effects of steel reinforcement corrosion on statically indeterminate reinforced concrete members. *Mater. Struct.* 49, 4959–4973.
- Golafshani, E.M., Rahai, A., Sebt, M.H., 2014. Bond behavior of steel and GFRP bars in self-compacting concrete. *Constr. Build. Mater.* 61, 230–240.
- Hasan Sahan Arel and Semsî Yazıcı, 2014. Effect of Different Parameters on Concrete-Bar Bond under High Temperature. *ACI Mater. J.* 111. <https://doi.org/10.14359/51686992>
- Kotynia, R., Szczech, D., Kaszubska, M., 2017. Bond behavior of GRFP bars to concrete in beam test. *Procedia Eng.* 193, 401–408.
- Lee, J.Y., Yi, C.K., Cheong, Y.G., Kim, B.I., 2012. Bond stress–slip behaviour of two common GFRP rebar types with pullout failure. *Mag. Concr. Res.* 64, 575–591.
- Lin, X., Zhang, Y., 2014. Evaluation of bond stress-slip models for FRP reinforcing bars in concrete. *Compos. Struct.* 107, 131–141.
- Maranan, G. B., Manalo, A. C., Karunasena, W., & Benmokrane, B. (2015). Pullout behaviour of GFRP bars with anchor head in geopolymer concrete. *Composite Structures*, 132, 1113-1121.
- Mias, C., Torres, L., Turon, A., Sharaky, I., 2013. Effect of material properties on long-term deflections of GFRP reinforced concrete beams. *Constr. Build. Mater.* 41, 99–108.
- Okelo, R., Yuan, R.L., 2005. Bond strength of fiber reinforced polymer rebars in normal strength concrete. *J. Compos. Constr.* 9, 203–213.
- Reichenbach, S., Preinstorfer, P., Hammerl, M., Kromoser, B., 2021. A review on embedded fibre-reinforced polymer reinforcement in structural concrete in Europe. *Constr. Build. Mater.* 307, 124946.
- Rolland, A., Argoul, P., Benzarti, K., Quiertant, M., Chataigner, S., Khadour, A., 2020. Analytical and numerical modeling of the bond behavior between FRP reinforcing bars and concrete. *Constr. Build. Mater.* 231, 117160.
- Solyom, S., Balázs, G.L., 2020. Bond of FRP bars with different surface characteristics. *Constr. Build. Mater.* 264, 119839.
- Tekle, B.H., Cui, Y., Khennane, A., 2020. Bond properties of steel and sand-coated GFRP bars in Alkali activated cement concrete. *Struct. Eng. Mech. Intl J.* 75, 123–131.